36th European Rotorcraft Forum - Paris, France, 7-9 September 2010

Paper 106

CFD analysis of Tilt-Rotor performance in steady flow

M.Biava[1], L.Vigevano[2]

[1] AgustaWestland Politecnico Advanced Rotorcraft Center (AWPARC), Milano, Italy. biava@aero.polimi.it

[2] Dipartimento di Ingegneria Aerospaziale, Politecnico di Milano, Italy. luigi.vigevano@polimi.it

Abstract

The ERICA tilt-rotor aircraft considered in the European project NICETRIP has been simulated in steady state conditions, both in the aircraft mode, with and without rotor, and in one conversion configuration, using a Navier-Stokes solver and a Chimera grid assembly. The comparison of the global aerodynamic coefficients with experimental data resulted in a limited success. The reasons of the underprediction of the drag coefficient are discussed.

1 Introduction

In recent years, the European rotorcraft industry has proposed the ERICA (Enhanced Rotorcraft Innovative Concept Achievement) concept, a tilt-rotor aircraft aimed at high operational performance levels and characterized by: i)a small rotor diameter, to allow for conventional aircraft-mode take-off and landing; ii) a tiltable outer portion of the wing, to reduce the downwash effect in helicopter-mode; iii) a structural continuity of the rotor tilting mechanism, to increase the structural safety. This initiative has been partially funded by the European Commission through several so-called Critical Technology Projects (the 6^{th} framework projects ADYN, TILTAERO, DART, to name a few) and through the presently running NICETRIP project, which specifically addresses the acquisition of new knowledge and technology validation concerning the tilt-rotor full design process.

Within NICETRIP, a 1/8 scale non powered model has been tested in the large wind tunnel facility at Politecnico di Milano to assess the aerodynamic coefficients in different configurations (aircraft-mode, several conversion-modes) without the influence of the rotor flow-field. In the present paper, the experimental data are compared with computations, performed with the CFD code ROSITA (ROtorcraft Software ITAly) [1], based on the solution of the Reynolds Averaged Navier-Stokes (RANS) equations coupled with the one-equation turbulence model of Spalart-Allmaras.

Different configurations of the tilt-rotor model are considered for the CFD simulations. To include the aerodynamic analysis of the transition corridor, different part of the aircraft (fuselage and main wing, movable outer wing and nacelle) are gridded independently and then assembled with a background grid within an overset (Chimera) grid system. Particular care has been taken to allow for sufficient grid overlap in the narrow regions between fixed and movable wing or between wing and nacelle.

The analysis has been carried out in two phases. First, the flow field around the unpowered model is computed for various attitudes of the tilt-wing and of the nacelle in the transition regime, for which the experimental data are available. Then, the propellers of the tilt-rotor are introduced into the CFD solution in a time averaged sense by means of the actuator disk model. The effects of the propellers are investigated by comparing the computed aerodynamic loads on the wing for the unpowered and powered models. Finally, in order to explain the underprediction of the computed drag, a new et of simulations are carried out with a refined grid and results are compared.

2 Solver description

The ROSITA solver numerically integrates the unsteady RANS equations, formulated in terms of absolute velocity and expressed in a rotating frame of reference linked to each blade, and supplemented with the Spalart-Allmaras turbulence model [6]. Additional source terms may eventually be introduced to apply the compressible vorticity confinement formulation [3], although this feature has not been employed in the present calculations. The equations are discretized in space by means of a cell-centred finite-volume implementation of the Roe scheme [5], formulated for a Chimera set of overlapped, multi-block structured grids. A high resolution scheme is obtained through the use of MUSCL extrapolation with a total variation diminishing (TVD) limiter to ensure monotone solutions. Time advancement is carried out with a dual-time formulation [4]. A 2^{nd} order backward differentiation formula was applied to approximate the time derivative and a fully unfactored implicit scheme is used in pseudo-time. The code is parallelized with a MPI paradigm.

3 Grid generation

Although only steady-state calculations are sought for, a full Chimera grid set [2] around the different components of the aircraft has been generated, so as to facilitate the simulation of the different geometrical configurations to be assessed. Independent multi-block grids have been produced around the fuselage and tail planes, the outer tiltable wing and the nacelle. A sample of the surface grids produced for these components is given in figure 1.

Particular care has been required to grid the narrow gaps located between fixed and tiltable wings and between the latter and the nacelle. The grid assembly need in fact to feature in these gaps, which thickness is of the order of 1 mm for the 1/8 scale model, a sufficient overlap so as to allow a successful Chimera tagging procedure. Also the background grid, representing the wind tunnel test section, features a strong clustering of grid points around the gaps. In turns, to limit the increase of the total number of grid points, the background grid cannot avoid to be highly non uniform close to the gap regions with non optimal values of the cell aspect ratios.

Figure 2 shows the generated grids, located so as to represent the aircraft mode configuration, referred later as TC45. The number of grid nodes for each component grid is given in table 1. The total number of control volumes of the considered grid set is about 10.3×10^6. The addition of the grid, employed to simulate the actuator disk, increase only slightly (0.2×10^6) this total amount. To simulate the conversion mode configuration, TC73, it has been sufficient to relocate the same grids within the background grid, as demonstrated in figure 3.

Fuselage	6268996
Tiltable wing	629790
Nacelle	1678745
Background	1724976
Total	10302507

Table 1: Number of control volumes for the different grids

4 Discussion of results

Test case	Re[%]	$Mach$[%]	α[deg] range	α_{tw}[deg]	α_n[deg]
TC45	9.68 $x10^5$	0.145	0 ÷4	0	0
TC73	7.80 $x10^5$	0.116	0 ÷6	15	60

Table 2: Geometrical and operating conditions

Two low-speed, moderate Reynolds number (Re), experimental conditions have been reproduced with the present calculations, see table 2, which specifies the geometrical configurations and the tunnel operating conditions. The incidences α, α_{tw} and α_n refer, respectively, to the complete aircraft attitude, to the inclination of the tiltable wing and to that of the nacelle. The test case TC45 refers to the aircraft mode configuration, while the test case TC73 is one of the possible tilted configurations which may occur during the conversion corridor of the vehicle. The comparison with the relevant experimental data will be carried out in the next subsection. The present computations do not consider the presence of the wind tunnel support and the blade stubs, mounted in front of

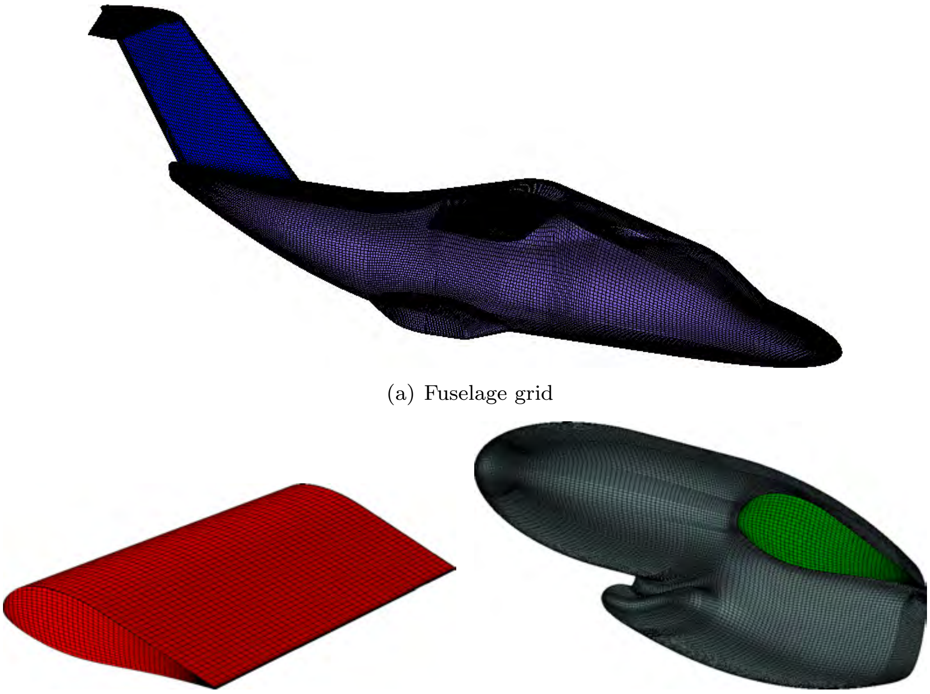

(a) Fuselage grid

(b) Tiltable wing grid

(c) Nacelle grid

Figure 1: Surface grids around different aircraft components

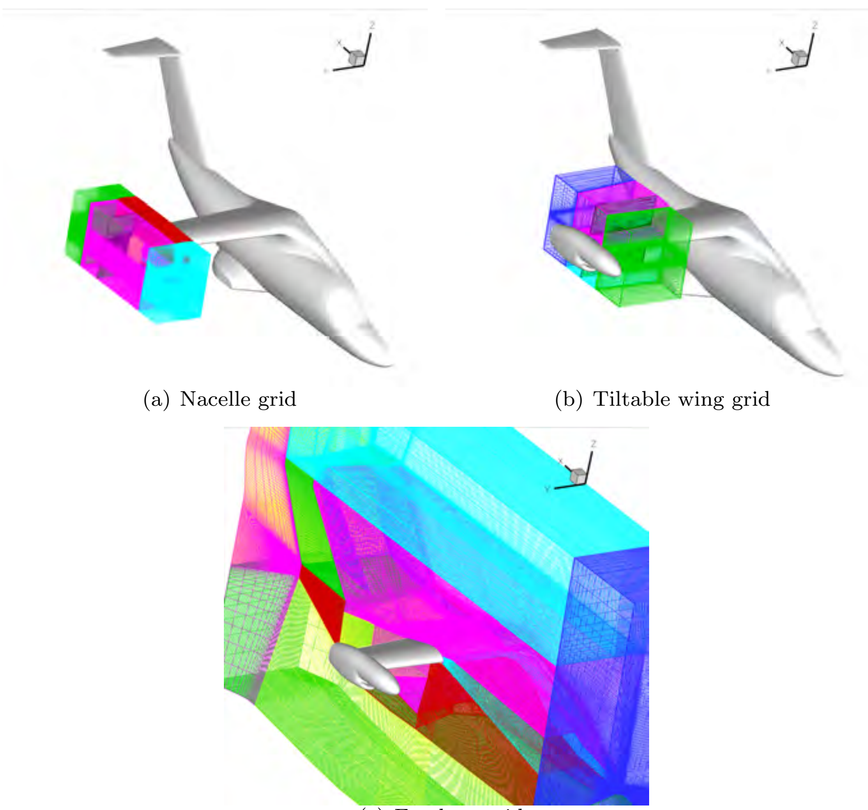

(a) Nacelle grid

(b) Tiltable wing grid

(c) Fuselage grid

Figure 2: Case TC45, aircraft mode

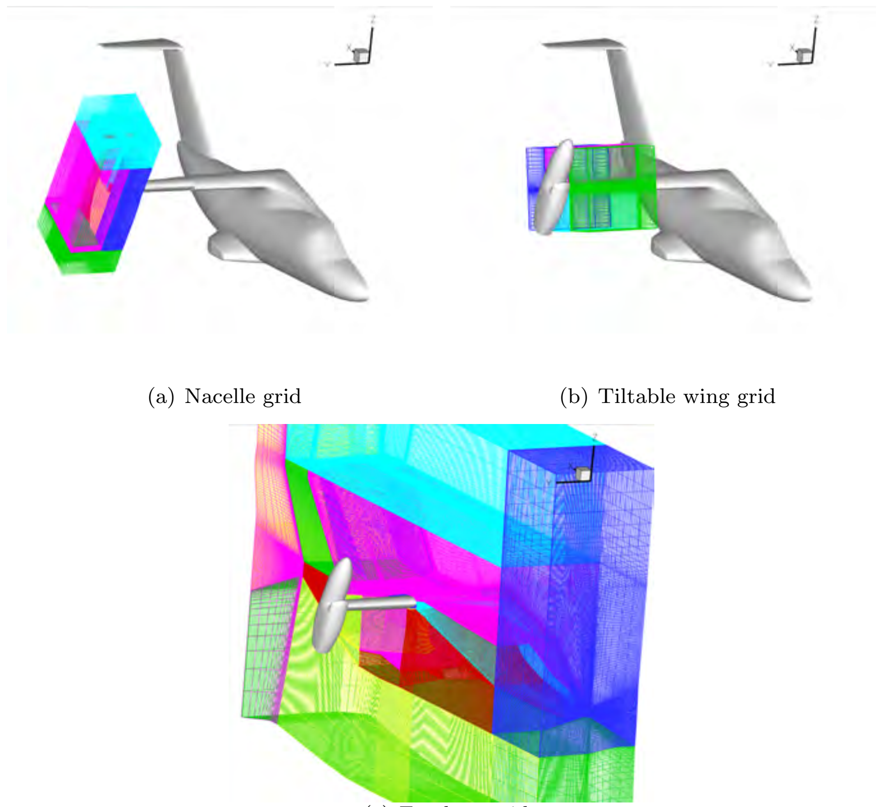

(a) Nacelle grid (b) Tiltable wing grid

(c) Fuselage grid

Figure 3: Case TC73, conversion mode

the nacelle during the tests: the experimental data are corrected accordingly. The correction for the blade stubes is accurate for TC45, but only approximate for TC73.

Few additional calculations in aircraft mode have been carried out considering the rotor as an actuator disk. These results will be compared with those computed *without* the rotor, to assess the influence of the rotor wake on the global loads.

4.1 Comparison with experimental data

For TC45, the predicted lift coefficient C_L compare favourably with the experiments, as shown in figure 4, where the normalized aerodynamic coefficients are plotted; normalization is carried out using the experimental values at $\alpha = 0$ as reference values. An exception is observed at the highest considered incidence, where the normalized error, computed as

$$\epsilon_{C_X} = \frac{|C_{X norm,num} - C_{X norm,exp}|}{C_{X norm,exp}}$$

reaches about 10 % (see table 3). On the opposite, the computed normalized drag coefficient C_D grossly underestimates the experimental data. Observing the agreement of C_L and the correct variation of C_D with incidence, one can argue that the induced drag is reasonably predicted while the simulation fails in computing the friction and form drag. Finally, the variation of the normalized pitching moment C_M with incidence is qualitatively well predicted, but with important quantitative differences (see fig. 4(c)).

α[deg]	ϵ_{C_L}[%]	ϵ_{C_D} [%]	ϵ_{C_M}[%]
0.01	1.91	62.88	12.71
2.00	2.38	56.90	98.78
4.01	9.70	48.70	36.91

Table 3: Relative error for the normalized aerodynamic coefficients, case TC45

A plot of the limiting stramlines on the aircraft surface (isolines for the tangential stresses), figures 5 and 6, shows a very smooth flow around the aircraft itself, with the exception of the nacelle wake.

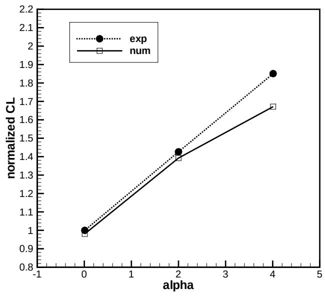

(a) Lift coefficient

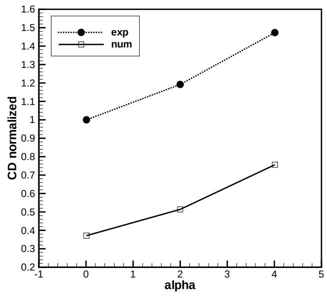

(b) Drag coefficient

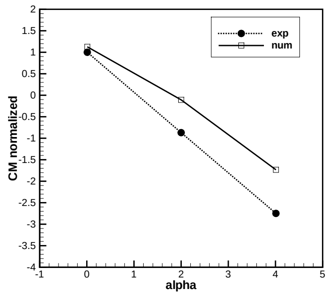

(c) Moment coefficient

Figure 4: Normalized aerodynamic coefficients versus incidence, case TC45

In particular, no clear separation is observed on the tail cone at the aft part of the fuselage, separation that was qualitatively observed using tufts during the wind tunnel campaign.

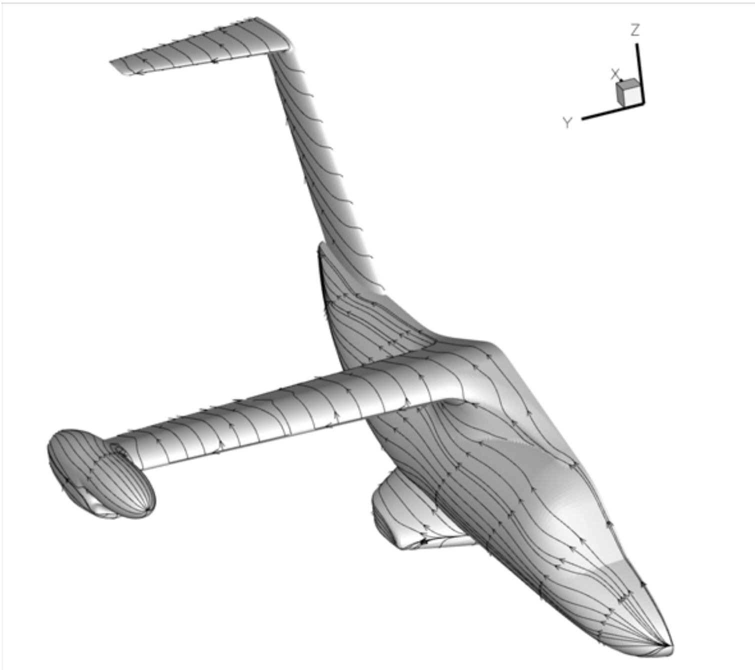

Figure 5: Limiting streamlines, case TC45, $\alpha = 4.01$ deg.

Very similar results are found for the conversion mode case, TC73 (see fig. 7). The flow around the nacelle is fully separated in this configuration, influencing the limiting streamlines on the tiltable wing. In figure 8 we can also observe how the relative inclination between fixed and tiltable wing produces what can be described as the influence of a vortical flow on the surface stresses. The presence of the nacelle wake is well evident in figure 9, which shows the distribution of stagnation pressure in different cross-planes behind the nacelle itself. In the same plot, is well evident the absence of flow separation from the fuselage, which causes the C_D underprediction.

4.2 Effects of the rotor in aircraft-mode

The actuator disk (AD) is located past the nacelle ogive (see fig. 10) and is represented with an annular grid in which a difference of pressure is imposed. The radial distribution of the pressure jump across the disk has been derived from previous European projects.

In absence of experimental results, the scope here is to compare the numerical calculation carried out in aircraft mode with and without AD, to asses its influence on the global loads. As shown by the normalized coefficients in figure 11, the presence of the AD increases both lift and drag coefficients, while inducing a pitch-down moment. Unfortunately the computed incidences are only two and this cannot allow to draw definite conclusions on the load trend with incidence.

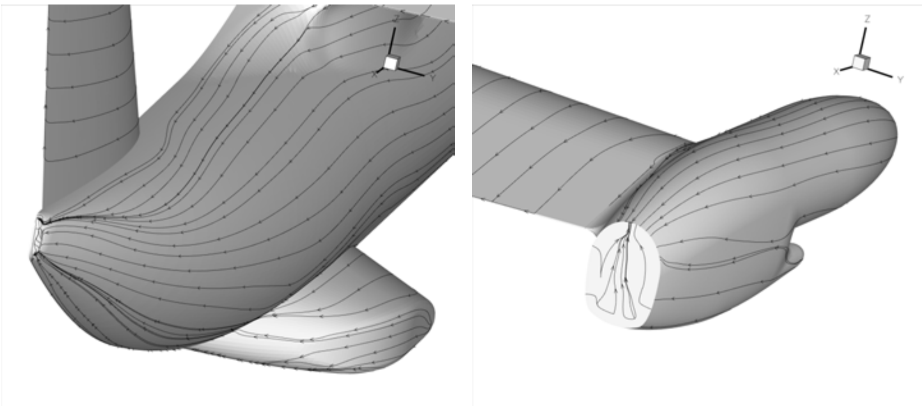

(a) Afterbody (b) Nacelle

Figure 6: Detail of the limiting streamlines on the afterbody and nacelle, case TC45, $\alpha = 4.01$ deg.

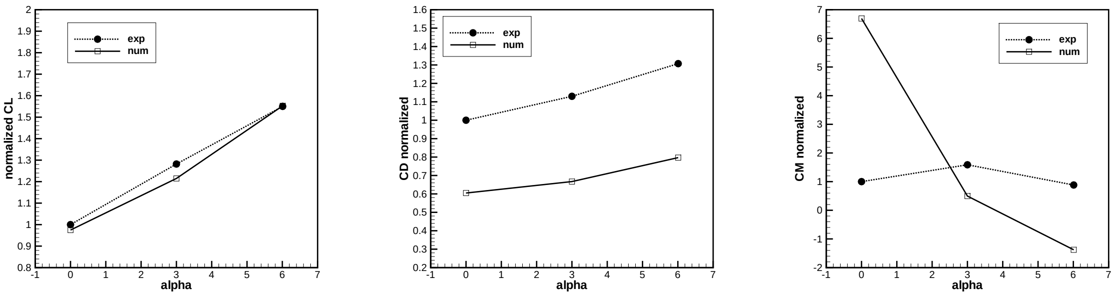

(a) Lift coefficient (b) Drag coefficient (c) Moment coefficient

Figure 7: Normalized aerodynamic coefficients versus incidence, case TC73

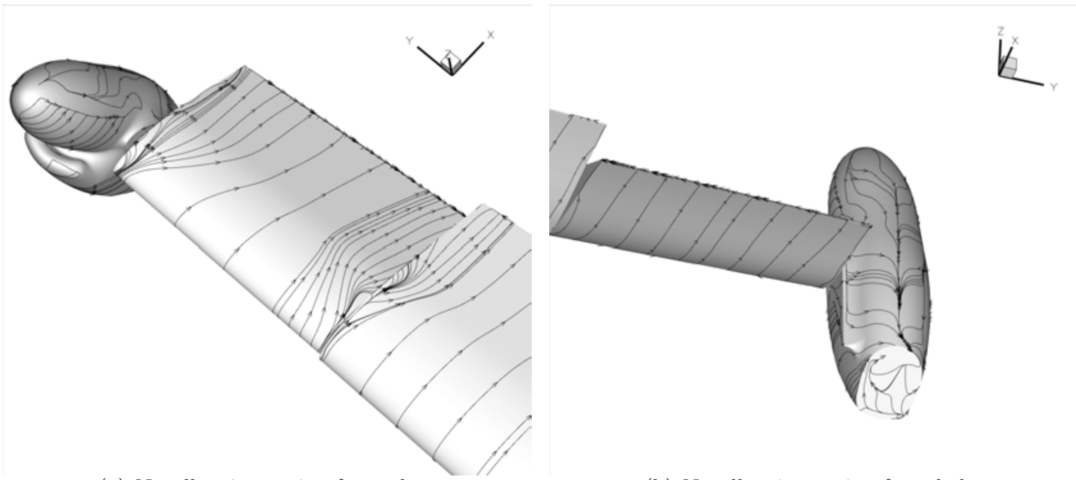

(a) Nacelle-wing region from above (b) Nacelle-wing region from below

Figure 8: Detail of the limiting streamlines on tiltable wing and nacelle, case TC73, $\alpha = 6.01$ deg.

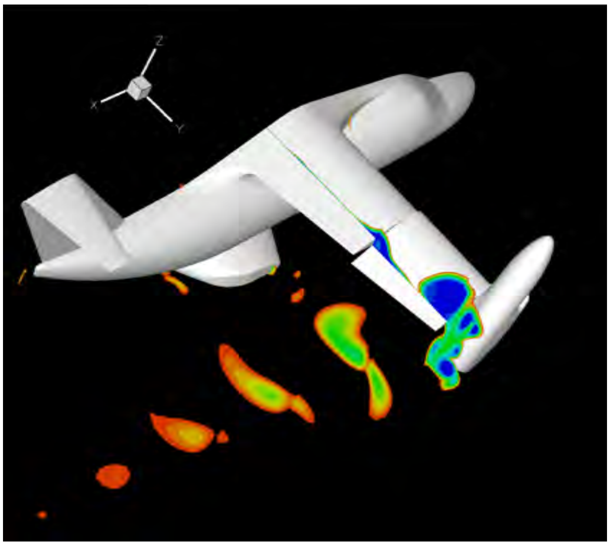

Figure 9: Stagnation pressure contours, case TC73, $\alpha = 6.01$ deg.

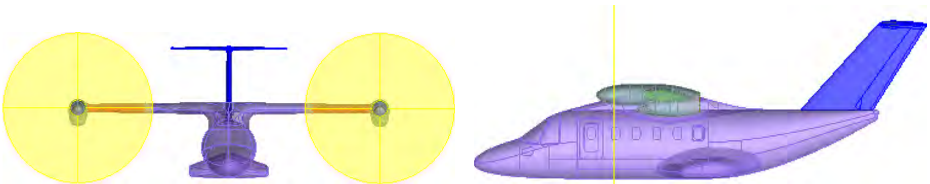

(a) Front view (b) Lateral view

Figure 10: Aircraft mode with actuator disk

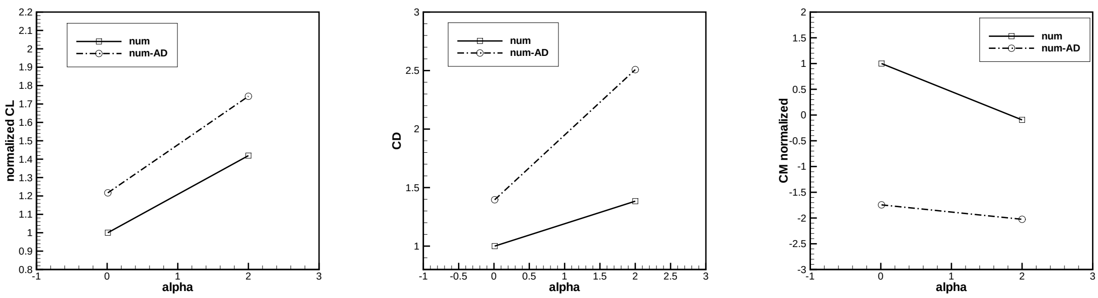

(a) Lift coefficient (b) Drag coefficient (c) Moment coefficient

Figure 11: Normalized aerodynamic coefficients versus incidence, case TC45 with actuator disk

4.3 Results with a refined grid

The investigation of the grid quality in the boundary layer regions showed few regions in which the dimensions of the cells located at the wall were too large, as evidenced from the y_+ distributions of the original grid, figure 12(a). This observation, together with the large drag underprediction, lead to a partial modification of the topology of the Chimera body grids and to a moderate grid refinement. The distribution of y_+ on the modified grid resulted appropriate (fig. 12(b)). The corresponding results in terms of normalized aerodynamic coefficients are shown in figure 13.

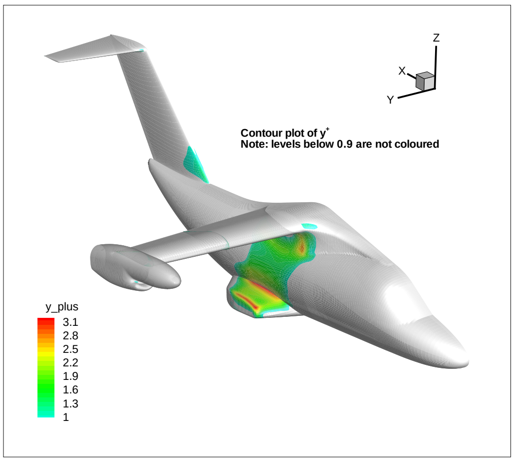

(a) Original grid

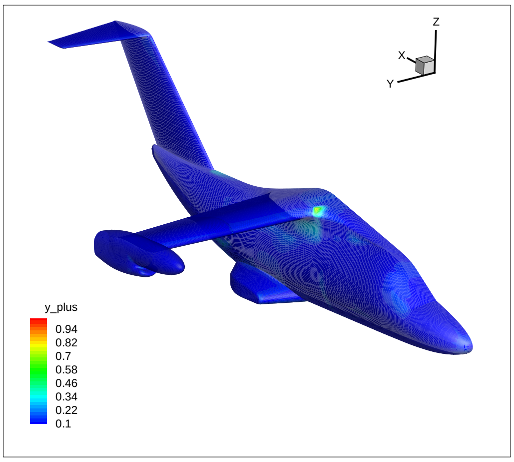

(b) Modified grid

Figure 12: Distribution of y^+ for the wall cells of the original and modified grids, case TC45, $\alpha = 4.01$ deg.

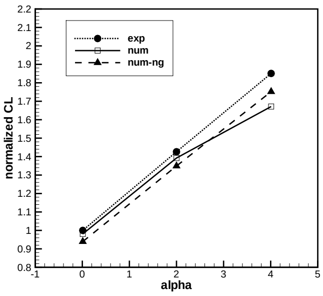

(a) Lift coefficient

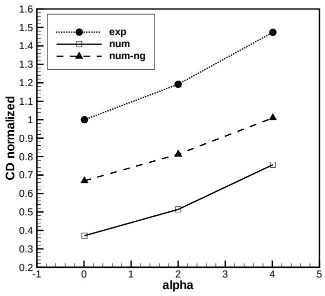

(b) Drag coefficient

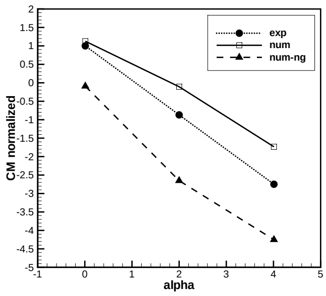

(c) Moment coefficient

Figure 13: Normalized aerodynamic coefficients versus incidence for the refined grid (dotted line), case TC45

α[deg]	ϵ_{C_L}[%]	ϵ_{C_D} [%]	ϵ_{C_M}[%]
0.01	6.06	33.11	109.18
2.00	5.42	31.81	205.00
4.01	5.34	31.46	54.66

Table 4: Relative error for the normalized aerodynamic coefficients with the refined grid, case TC45

Referring also to table 4, the following comments can be done: i) a slight increase in the C_L error occurs, which is more uniform at all angle of attack, suggesting that a correction of the nominal incidence should have been considered; ii) a considerable increase in normalized C_D is observed, which still do not allow for a good comparison with the experimental values, since the three-dimensionl separation in the aft fuselage is not well predicted, see fig.14 ; iii) large variations in the normalized C_M may be observed.

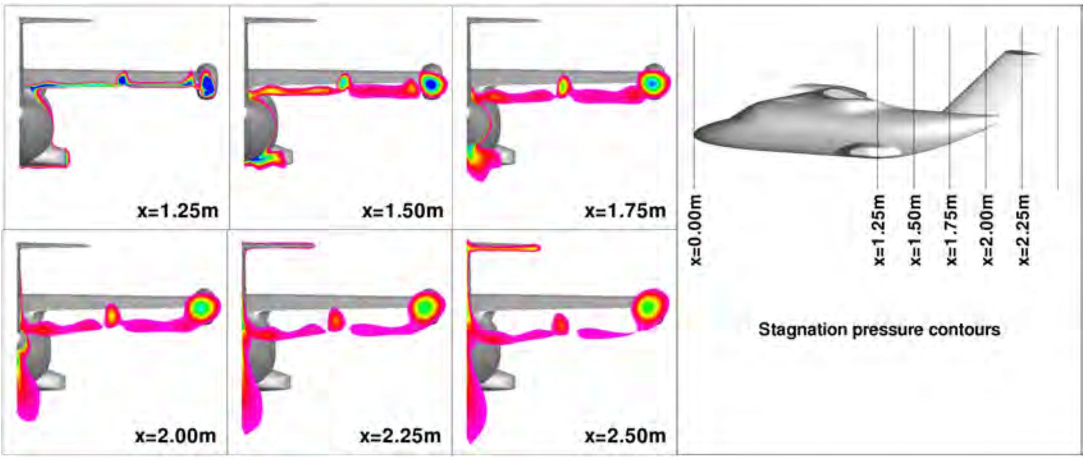

Figure 14: Total pressure distribution at different cross-planes, refined grid, case TC45, $\alpha = 4.01$ deg.

5 Conclusions

The tilt-rotor aircraft considered in the European project NICETRIP has been simulated in steady state conditions using a Navier-Stokes solver and a Chimera grid assembly. The use of an overset grid system has allowed, with a limited grid generation effort, to examine two different geometrical configurations, namely the aircraft mode and one conversion mode. The latter represents a particular complex geometry, due to the relative inclination between the fixed portion and the tiltable portion of the wing and between the latter and the nacelle. The simulations allowed for a detailed examination of the complex flow fields around the aircraft, in particular for the conversion mode where massively separated flow appears at the fixed/moving wing junction and at the wing/nacelle junction.

The limited comparison of the numerical and experimental global aerodynamic coefficients, carried out without the presence of the rotor, has however shown that the drag coefficient predicted by the ROSITA code is largely underpredicted. While the the induced drag seems correctly estimated, the viscous and form drag is not. The main reason for this is the failure in reproducing the flow separation at the tail cone of the fuselage. It is customary in these occasions to blame the turbulence model. In fact, the moderate Reynolds number at which the simulations have been performed do not match with the hypothesis that underlie the Spalart-Allmaras model. The other reason for not reproducing the flow separation at the rear fuselage could be an insufficient grid density in the boundary layer region. A refined grid has been has been generated to assure that the first grid spacing close to the solid surface is well inside the laminar sublayer: the calculations carried out with such a grid allow to improve the computed drag results but not to the extent of matching the experimental data.

Finally, the steady state actuator disk model has been successfully employed to represent the rotor/wing interference.

Aknowledgements: this work has been partially carried out under the EC supported FP6/Aeronautics Project AIP5-CT-2006-03-944 NICETRIP.

References

[1] M. Biava. *RANS computation of rotor/fuselage unsteady interactional aerodynamics*. PhD thesis, Politecnico di Milano, 2007.

[2] M. Biava, J.-C. Boniface, and L. Vigevano. Influence of wind-tunnel walls in helicopter aerodynamics predictions. In *31st European Rotorcraft Forum, Firenze, Italy*, 2005.

[3] M. Biava and L. Vigevano. Assessment of the vorticity confinement technique applied to rotorcraft flows. In *42nd AIAA Applied Aerodynamics Conference, Orlando, FL. AIAA 2003-3524*, 2003.

[4] A. Jameson. Time dependent calculations using multigrid with applications to unsteady flows past airfoils and wings. In *10th AIAA Computational Fluid Dynamics Conference, Honolulu, HI. AIAA 91-1596*, 1991.

[5] P.L. Roe. Approximate riemann solvers, parameter vectors and difference schemes. *J.Comput. Phys*, 43:357–372, 1981.

[6] P.R. Spalart and S.R. Allmaras. One equation model for aerodynamic flows. In *30th AIAA Aerospace Science Meeting & Exhibit, Reno, NV. AIAA 92-0439*, 1992.